Available online at www.sciencedirect.com
ScienceDirect
Polymer 47 (2006) 8163–8172
polymer
www.elsevier.com/locate/polymer

Morphology, reorganization and stability of mesomorphic nanocrystals in isotactic polypropylene

Qamer Zia [a], René Androsch [a,*], Hans-Joachim Radusch [a], Stefano Piccarolo [b]

[a] *Martin-Luther-University Halle-Wittenberg, Center of Engineering Sciences, D-06099 Halle/Saale, Germany*
[b] *University of Palermo, Department of Chemical Engineering, 90128 Palermo, Italy*

Received 22 July 2006; received in revised form 29 August 2006; accepted 20 September 2006
Available online 11 October 2006

Abstract

The morphology and thermodynamic stability of crystals of isotactic polypropylene (iPP) were analyzed as a function of the path of crystallization by atomic force microscopy (AFM) and differential scanning calorimetry (DSC). Samples were melt-crystallized at different rates of cooling using a ''controlled rapid cooling technique'', and subsequently annealed at elevated temperature. Mesomorphic equi-axed domains with a size less than 20 nm were obtained by fast cooling from the melt at a rate larger about 100 K s^{-1}. These domains stabilize on heating by growing in chain direction and cross-chain direction, to reach a maximum size of about 40–50 nm at a temperature of 433 K, with the quasi-globular shape preserved. Annealing at 433 K additionally triggers formation of different types of lamellae. It is suggested that these lamellae either develop by coalescence of nodules, or by recrystallization from the melt. The transition from the disordered mesomorphic structure, evident at ambient temperature after fast crystallization, to monoclinic structure on heating at about 340 K occurs at local scale within existing crystals, and cannot be linked to complete melting of mesomorphic domains and recrystallization of the melt. The temperature of melting of initial mesomorphic domains, after reorganization at elevated temperature, is identical to the temperature of melting of rather perfect lamellae, obtained by initial slow melt-crystallization, followed by annealing. The close-to-identical temperatures of melting of these crystals of largely different shapes are confirmed by model calculations, using the Gibbs–Thomson equation. Modeling of the melting temperature reveals that nodular crystals, stabilized by annealing at high temperature, exhibit a similar fold-surface as lamellar crystals.

Keywords: Isotactic polypropylene; Crystal morphology; Crystallization

1. Introduction

The morphology of crystals in semi-crystalline polymers is controlled by the chemical architecture of the macromolecule and by the condition of crystallization. Macromolecules can form extended-chain crystals, folded-chain lamellae, or fringed micelles, and intermediate crystal forms. Extended-chain crystals exhibit the lowest free enthalpy of all possible crystal morphologies, however, full extension of the chain as prerequisite for the formation of an extended-chain crystal requires a large activation energy, and is therefore not obtained on crystallization from the quiescent and entangled melt [1,2]. The formation of laterally extended lamellae by chain folding involves reduced activation energy and can be considered as typical crystal morphology in semi-crystalline polymers [3–5]. Chemical irregularities, like branches in polyethylene [6], or disturbance of the crystallization process by variation of temperature or extreme super-cooling may hinder adjacent back-folding of the macromolecule for the generation of a perfect fold-surface and cause a reduction of the lateral dimensions of crystals. In extreme cases formation of fringed micelles occurs. These are characterized by macromolecules which frequently leave or enter the crystal, i.e., one molecule participates in more than one crystallite [7,8]. The basal plane of fringed micelles has an increased specific surface free energy, compared to folded-chain lamellae or extended-chain crystals, and therefore fringed micelles are thermodynamically not favored [9].

* Corresponding author. Tel.: +49 3461 46 3762; fax: +49 3461 46 3891.
E-mail address: rene.androsch@iw.uni-halle.de (R. Androsch).

0032-3861/$ - see front matter © 2006 Elsevier Ltd. All rights reserved.
doi:10.1016/j.polymer.2006.09.038

This paper focuses on the condition of formation of non-lamellar mesomorphic nanocrystals on melt-crystallization in isotactic polypropylene (iPP), and the evaluation of the stability of these nanocrystals by analysis of structural changes on heating.

The morphology of mesomorphic domains in quenched iPP was directly evaluated by transmission and scanning electron microscopy [10–14]. Further studies employed line-broadening analysis of wide-angle X-ray scattering reflections [15,16], or analysis of the small-angle X-ray scattering [17,18]. The shape of the mesomorphic domains, developed by quenching, is consistently described as being nodular. Reports about the size of the domains differ slightly, probably caused by the quenching technique and the particular iPP grade used for the study. Ultra-quenching of films of thickness 100 nm to a temperature lower than the glass transition temperature of the mobile amorphous phase, which is reported to be about 253–258 K [10,11,14] or 243 K [17], produces structures of size smaller than 2.5 nm [10]. Subsequent heating to room temperature revealed nodules of size ranging from 7.5 nm to 10 nm [10], i.e., the initial small domains increase in size on heating above the glass transition, which, in turn, increases to about 274 K [17]. The size of nodules of 10 nm at ambient temperature was reproduced by preparing a 0.25 mm thick film of mesomorphic iPP using melt-extrusion on a chill roll at a temperature of 281 K [12]. In a different study, iPP films of thickness between 0.10 and 0.15 mm were quenched from the melt into ice-water, producing equi-axed domains of size of about 20 nm [13]. Finally, quenching of a 14 μm thick film in an ethanol/dry ice mixture yielded micro-crystalline regions of 10–20 nm size [14]. Summarizing microscopic data available in the literature, it can be concluded that the size of the domains in quenched samples is about 10–20 nm at ambient temperature, being consistent with X-ray data, which point to a size of nodules between 3 nm [15] and about 5 nm [16]. The fraction of mesomorphic phase depends on the rate of cooling and increases continuously between 10 and 100 K s^{-1} from zero to a maximum value of about 30%, mainly at the expense of monoclinic α-structure [19,20].

Recently, high speed calorimetry was employed to determine the temperature of melt-crystallization of iPP as a function of the rate of cooling [21–23]. It was found that the monoclinic α-phase forms at relatively high temperature between about 390 K on slow cooling at 0.02 K s^{-1} and about 350 K on fast cooling at 120 K s^{-1}. Application of an even higher cooling rate completely suppressed the formation of monoclinic α-structure. Cooling at a rate between 70 and 300 K s^{-1} revealed a second exothermic event at a temperature lower than 315 K, which was assigned to the formation of the mesophase. Finally, cooling at rates faster than 1000 K s^{-1} even disabled mesophase formation. Accordingly, two separate crystallization events at largely different temperatures are detected on cooling at rates between 70 and 120 K s^{-1}.

The molecules within the mesomorphic domains exhibit a 3_1 helical conformation, which is identical to the chain conformation in the α-crystalline phase. Packing is less dense and the unit cell parameters in inter-helical direction are increased in the mesomorphic structure. The literature suggests helix reversals as major reason for the increased inter-chain packing, i.e., a random occurrence of left-handed and right-handed helices [14,24,25]. The mesomorphic structure starts to reorganize by rewinding of helices on heating into the monoclinic α-structure at a temperature of about 330–340 K [26,27]. The reorganization of the initial nodular crystal morphology after quenching, evident at ambient temperature, in order to achieve a state of lower free enthalpy, includes an increase of the size from about 10 nm to about 20–30 nm at a temperature of 413 K, with the initial geometry unchanged [10,13], being in agreement with WAXS data [13,16]. Annealing at an even higher temperature, or for an extended period of time at 413 K, apparently causes a change of the crystal shape since lamellae were observed [10,12,13]. There are indications that the grown domains either partially aggregate to lamellae [10] or lamellae grow as a result of a conventional secondary crystallization process [12]. The exact mechanism of lamellae formation by reorganization of initial mesomorphic nodules on heating above 413 K is not fully explained yet.

The present study is the continuation of recently performed investigations about the effect of the crystal morphology on the degree of reversible melting in iPP [28,29]. Samples were slowly cooled or quenched from the melt, and subsequently the morphology was investigated by atomic force microscopy (AFM). The images revealed, as expected, lamellar crystals for the slowly cooled preparation, and nodular domains for the quenched sample. Additional annealing at 423 K did not change the structure qualitatively, rather resulted in an increase of the crystal dimensions for both the lamellar and the nodular crystals. Thermal analysis revealed close-to-identical melting temperatures for these crystals of strongly different shapes and sizes, which, however, were not expected, and are addressed in the present study.

Summarizing the scope of the present paper, we intend to further analyze the reorganization behavior and therefore the thermodynamic stability of initial small and mesomorphic crystals of iPP, in order to provide detailed and quantitative information for controlling the semi-crystalline structure and therefore the properties of iPP.

In the first part of this paper we focus on the evolution of the crystal morphology as a function of the condition of melt-crystallization. Subsequently the reorganization of initial crystals on annealing at elevated temperature is explored. This part includes a discussion of the phase transition from the mesomorphic to the monoclinic phase at about 340 K, from point of view of the crystal morphology. In the last part of this study, the melting behavior of crystals of largely different morphology, as obtained by melt-crystallization along different routes, is analyzed by calorimetry, and discussed in terms of the Gibbs–Thomson equation.

2. Experimental

2.1. Materials

We used an iPP with a mass-average molar mass and polydispersity of 373 kg mol^{-1} and 6.2, respectively, provided by

Montell Polyolefins. The melt-flow rate is 3.3 g (10 min)$^{-1}$, determined at 503 K with a load of 2.16 kg [30]. A series of specimens were prepared using a special device for controlled rapid cooling, developed by Piccarolo et al. [31]. The instrumentation allows cooling of films up to a maximum rate of about 2000 K s^{-1}. Pre-shaped films of thickness of 100 μm were sandwiched between glass, aluminum foil and metal plates, with a thermocouple placed between the aluminum and the metals plates. The glass slides served for generation of a sufficiently smooth surface for AFM analysis. The samples were heated to 473 K, held for 5 min, in order to erase the thermal history, and subsequently cooled to 288 K, which was the temperature of the coolant. A wide variety of samples of different structures were prepared by varying the effective rate of cooling between 10^1 and 10^3 K s^{-1}, controlled by the flux of water used to spray the sandwich. From the slope of the recorded non-linear cooling curves, temperature versus time, an effective cooling rate was estimated at a temperature of 343 K. Annealing of samples was done using a Leitz hot-stage 1350, in combination with a Rheometric Scientific temperature controller. The samples were heated to the annealing temperature at a rate of 10 K min^{-1}, the annealing time was 60 min, and subsequent cooling to ambient temperature was done at a rate of 10 K min^{-1}.

2.2. Instrumentation

2.2.1. Microscopy

Direct analysis of the crystal morphology was done using a Quesant Q-Scope 250 AFM, equipped with a 40 μm × 40 μm scanner. Images were taken with standard silicon cantilevers NSC 16, operating in tapping mode. The resonant frequency of the cantilever is about 170 kHz, and the force constant is 40 N m^{-1}. AFM images were collected at ambient temperature. Additional information about the superstructure is gained by polarizing optical microscopy, using a Leica DMRX microscope, equipped with a Leitz hot-stage 1350, and full periphery for automated data acquisition in dynamic experiments as a function of temperature.

2.2.2. Density

The density, ρ, of the initial preparations was measured at a temperature $T_0 = 288$ K with a density gradient column, using a mixture of water and ethanol. The minimum and maximum detectable densities, controlling the resolution, were approximately 0.8840 and 0.9055 g cm^{-3}, respectively. The measured density data were extrapolated to ambient temperature–density data using Eq. (1):

$$\rho(T) = \frac{1}{1/\rho(T_0) \times (1 + \alpha_{\text{thermal}} \Delta T)} \tag{1}$$

α_{thermal} is the linear thermal expansion coefficient and ΔT is the temperature difference between measured and extrapolated temperature. For the calculation we used a thermal expansion coefficient of 1.05×10^{-4} K^{-1} [32].

2.2.3. Wide-angle X-ray diffraction (WAXS)

WAXS data were collected on a diffractometer URD 63 from Seifert-FPM, using Ni-filtered Cu Kα radiation (wavelength 0.15418 nm), and a scintillation counter for registration. Measurements were done in symmetric transmission mode.

2.2.4. Differential scanning calorimetry (DSC)

Thermal analysis was done with a DSC 7 from Perkin–Elmer, equipped with the cryogenic cooling accessory CCA 7. The furnaces were purged with nitrogen gas at a flow rate of 40 mL min^{-1}. The instrument was calibrated with respect to temperature and heat-flow rate using standard procedures [33]. Heat-flow rate raw data were corrected for instrumental asymmetry by subtraction of a baseline, measured under identical conditions as the sample run, including matched masses of the aluminum pans, used for encapsulation of the samples. Samples with a mass of about 1 mg were placed in 20 μL aluminum pans obtained from Mettler–Toledo. The rates of heating and cooling in all experiments were 20 K min^{-1}.

3. Results

3.1. Initial structure

Fig. 1a shows the density of polypropylene at 298 K as a function of the effective rate of cooling at a temperature of 343 K, and Fig. 1b the corresponding wide-angle X-ray scattering of the samples of different density and history of crystallization. The data in Fig. 1 allow to establish a cooling rate – macroscopic density – structure relation. Specimens cooled at a rate higher than 80 K s^{-1} exhibit a density of almost 0.89 g cm^{-3} and do not show evidence of monoclinic α-structure in the X-ray scans. The X-ray data rather show two halos which can be assigned to mesomorphic iPP. The mesomorphic structure is completely replaced by monoclinic α-structure if the cooling rate is decreased to a value of about 20 K s^{-1}, or lower. Application of an intermediate rate of cooling between 20 and 80 K s^{-1} results in coexistence of α-monoclinic and mesomorphic crystals, in addition to the amorphous phase. The density measurements and X-ray data reveal that a large variety of phase structures can be generated by variation of the cooling rate on melt-crystallization. Next, the crystal morphology of these samples is evaluated by AFM, focussing on the detection of non-lamellar structures which were not systematically studied yet. Fig. 2a shows AFM images of selected samples which were crystallized from the melt at a cooling rate of 22, 50, 80, 165, 450 and 1050 K s^{-1}. The scan area is 1 μm × 1 μm. Fig. 2b shows enlargements of the images obtained on samples cooled at 22 and 1050 K s^{-1}. The image size is, in this case, 500 nm × 500 nm. Samples which were cooled at a rate between 6 and 50 K s^{-1} show coexistence of lamellae and nodules. The thickness of lamellae is about 10–15 nm, and the apparent diameter of the nodules is about 20 nm. Note that there is no evidence that nodules are truly spherical, which would allow to define a diameter. For this reason the term *apparent* diameter for quantification of the size of nodules is introduced. Increasing the rate of cooling

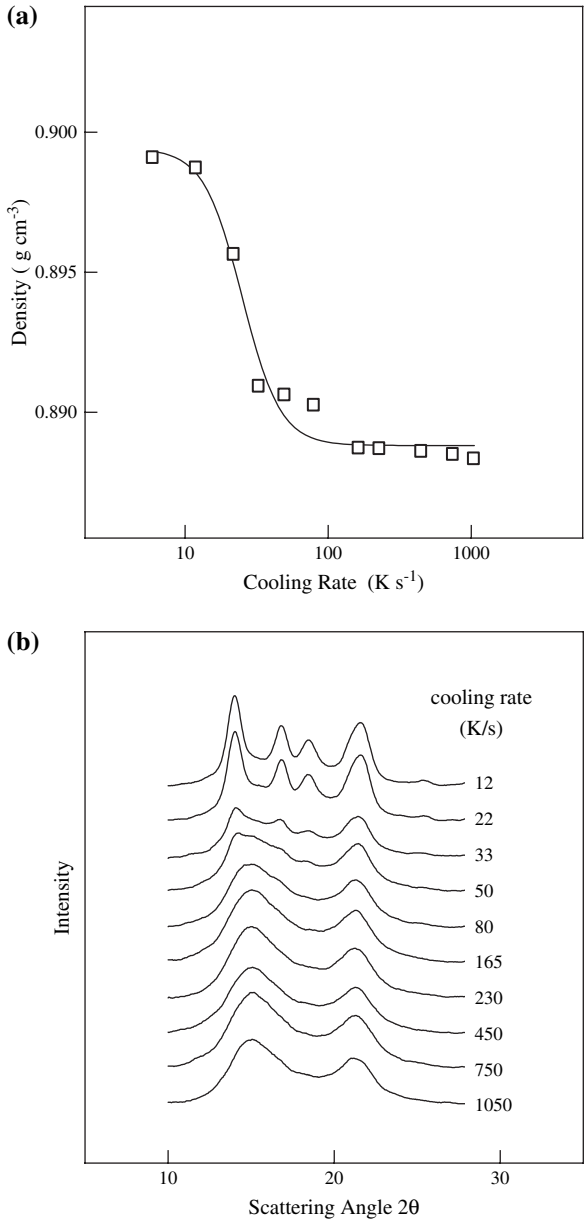

Fig. 1. (a) Density of iPP at 298 K as a function of the rate of cooling. (b) WAXS of iPP, crystallized at different rates of cooling from the melt.

to 80 K s^{-1}, or faster, completely suppresses the formation of lamellae. The size of nodules is almost independent on the rate of cooling. The estimation of the apparent diameter points to a slight decrease from about 20 nm to 15 nm on increasing the rate of cooling from 50 to 1050 K s^{-1}. Fig. 2c shows the optical micrographs of samples which were cooled at 22, 165 and 1050 K s^{-1}, in order to gain information about the superstructure at the micrometer scale. The scaling bar corresponds to 30 μm. The sample which was crystallized at a cooling rate of 22 K s^{-1} shows a space-filling spherulitic superstructure with a bimodal distribution of the spherulite size. The diameter of the larger spherulites is of the order of 50 μm, and the size of the remaining spherulites is considerably decreased. The dual population of spherulites consistently goes parallel with the observation of a mixed lamellar–nodular nanostructure (Fig. 2a and b). Samples crystallized at a rate faster than 50 K s^{-1} show at best only a few small isolated spherulites, which are embedded in a weakly birefringent matrix. These observations confirm earlier investigations [34], and are now related to the structure at the nanometer scale.

Table 1 summarizes the observations regarding crystal shape and size, internal crystal structure, and superstructure, as derived from the results shown in Figs. 1 and 2. Most striking is the relation between the crystal shape, internal symmetry of crystals, and the superstructure. The data suggest that lamellae exhibit a monoclinic internal symmetry, and that nodules exhibit a mesomorphic arrangement of chains. Nodular crystallization, obviously, is not connected with the formation of spherulites. The data in Figs. 1 and 2 show that non-isothermal melt-crystallization of iPP allows formation of largely different phase morphologies. Slow cooling of the melt, or isothermal crystallization above about 373 K triggers formation of laterally extended, in shape anisotropic, folded-chain lamellae with monoclinic arrangement of molecules [35,36]. Fast cooling leads to the formation of mesomorphic domains of quasi-isotropic shape and reduced size of 20 nm or less. Coexistence of both extremes is possible. The thermodynamic stability is evaluated next by the analysis of the structure as a function of temperature.

3.2. Reorganization on annealing at elevated temperature

Fig. 3a shows AFM images of iPP melt-crystallized at 22 (top) and 165 K s^{-1} (bottom), representing preparations with a lamellar–nodular and an exclusively nodular structure. The left images show the initial structure, as is observed after melt-crystallization at the indicated rate of cooling. The images to the right were collected after annealing at 413, 423, and 433 K for a period of 60 min. Note that the images were taken at ambient temperature, i.e., after annealing the samples were cooled at a rate of 10 K min^{-1} to room temperature for AFM analysis. The lamellar–nodular structure of the sample, which was initially melt-crystallized at 22 K s^{-1} is preserved on heating and annealing. The size of the crystals changes only slightly on heating to 403 K and subsequent annealing at identical temperature. Further increase of the temperature to 433 K is connected with a drastic increase of the crystal dimensions. This includes the thickness of lamellae as well as the apparent nodule diameter. Similarly the nodule size of the sample, which was initially melt-crystallized at a rate of 165 K s^{-1}, increases only slightly on heating and annealing at 403 K. Also in this case the nodule size increases drastically on heating to 433 K. Fig. 3b shows estimates of the apparent nodule size of the samples, which initially were crystallized at different rates of cooling, as a function of the annealing temperature. The line serves for guiding the eye, and is not a fitted function, or related to a specific data set. The initial apparent nodule size is close to 20 nm, increases to 20–25 nm at an annealing temperature of 403 K, and then approaches about 40 nm on annealing at 433 K. The sample which was initially melt-crystallized at a rate of 1050 K s^{-1} is an exception.

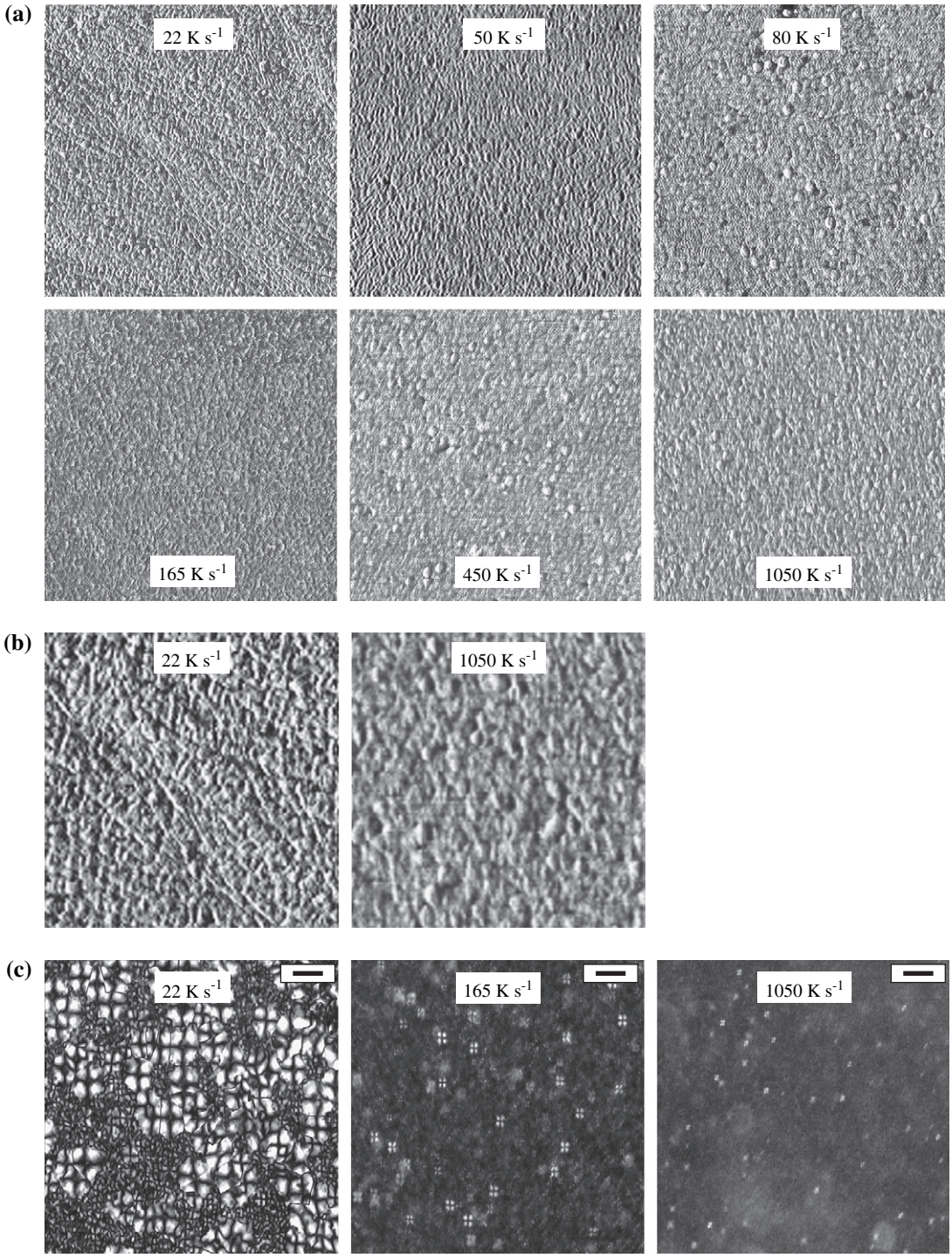

Fig. 2. (a) AFM images of iPP, melt-crystallized at 22, 50, 80, 165, 450 and 1050 K s^{-1} cooling rate. The image size is 1 μm × 1 μm. (b) Soft zoom of AFM images of iPP, melt-crystallized at 22 (left) and 1050 K s^{-1} (right) cooling rate. The image size is 0.5 μm × 0.5 μm. (c) Optical micrographs of iPP, melt-crystallized at 22 (left), 165 (center) and 1050 K s^{-1} (right) cooling rate. The scaling bar corresponds to 30 μm.

Annealing at 433 K triggered the formation of lamellae of different types, which are shown in Fig. 3c. The size of both the images is 1 μm × 1 μm. The left image shows lamellae, which seem composed of former nodules. This conclusion is derived from the distinct blocky internal structure of the lamellae. A different type of lamellae is shown with the right image. In this case internal surfaces were not detected by AFM. Furthermore, we note coexistence of these lamellae with nodules of rather large size. Apparently the formation of these different types of lamellae occurred along different thermodynamic pathways, which is shown schematically in Fig. 3d. Heating to 433 K causes melting of small and therefore less stable nodular crystals. The remaining large nodules may coalesce to lamellae for the reduction of the surface energy, as is shown at the bottom left illustration in Fig. 3d. Alternatively, there is possible conventional melt-recrystallization which yields

Table 1
Crystal shape, crystal size, crystal structure and superstructure of melt-crystallized iPP as a function of the rate of cooling

Cooling rate ($K\,s^{-1}$)	Crystal shape	Crystal dimension (nm)	Crystal structure	Superstructure
6–50	Lamellar nodular	Lamellae thickness: 10–15, nodule size: 20	Monoclinic mesomorphic	Spherulitic bimodal size distribution
80–1050	Nodular	20, slightly decreasing with increasing cooling rate	Mesomorphic	Non-spherulitic weakly birefringent

formation of lamellae, within a matrix of large nodules and amorphous structure.

In addition the superstructure at the micrometer scale was monitored by optical microscopy. Annealing does not cause a change of the superstructure. The bimodal size distribution of spherulites of samples initially melt-crystallized at a rate less than 50 $K\,s^{-1}$ is preserved on annealing. In samples melt-crystallized at higher rate, few isolated spherulites, formed on initial melt-crystallization, are still evident after annealing.

3.3. Thermodynamic stability of lamellar and nodular crystals of iPP

We assume at present that the stability of the originally grown crystals cannot be evaluated with standard DSC experimentation, since the usually applied low rate of temperature-change of $<10^2\,K\,min^{-1}$ permits reorganization on heating. Crystal reorganization may be suppressed in fast-scanning calorimetry, which was already used to evaluate the crystallization behavior of iPP [21,22]. The thermodynamic stability of crystals of iPP of largely different geometry is estimated within the present study by the temperature of melting. Samples, which contained at ambient temperature lamellar and nodular crystals after melt-crystallization were heated to 433 K, isothermally annealed for a period of 60 min, cooled to 298 K at a rate of 20 $K\,min^{-1}$, and finally melted at identical rate of temperature-change by heating to 473 K. The entire thermal treatment, except the initial melt-crystallization, was done in the DSC furnace. The annealing temperature of 433 K is not chosen arbitrarily, rather was selected such that reorganization between the annealing temperature and final melting is minimized, or even completely suppressed. With this assumption, a direct relation between crystal morphology and melting temperature can be established, which is the intention of the experiment, in order to estimate the thermodynamic stability of crystals of different shape. The upper two curves in Fig. 4 show the approach of the annealing temperature at 433 K. The thin and thick lines represent the samples with lamellar and nodular crystals. The lower two curves show the final melting after annealing at 433 K, and cooling to 298 K. The sample which contains lamellar and monoclinic crystals as a result of the primary melt-crystallization is characterized by the absence of phase transitions on heating to the annealing temperature of 433 K (thin line). The heating scan of the sample, which initially contains nodular and mesomorphic domains (thick line), indicates reorganization, including the phase transition from the mesomorphic structure to the monoclinic structure, starting at about 340 K, as is frequently described in literature [26,27]. The melting of the initial crystal starts at about 410–415 K (see arrow in Fig. 4), regardless the initial crystal structure and crystal morphology. The observation of large-scale reorganization on heating above 415 K by DSC is consistent with the large increase of the crystal size, discussed in Fig. 3b. The melting temperatures of both preparations are nearly identical even without annealing. After annealing, the samples were cooled to ambient temperature, in order to simulate the temperature–time profile of the samples which were analyzed by microscopy. It is not expected that cooling and reheating of the annealed samples, at least up to the temperature of annealing, cause further irreversible structural changes. Heating of the reorganized structures (lower two curves) proves close-to-identical temperatures of melting of both preparations, indicating similar thermodynamic stability of crystals of different morphology, formed along different thermodynamic pathways. The difference between the maxima of the melting peaks, which are located at about 446 K, is less than 1 K.

4. Discussion

The present study concerns the analysis of the morphology and thermodynamic stability of the crystalline phase of melt-crystallized and subsequently annealed iPP at elevated temperature. This research is considered as a continuation of the long-standing effort regarding an in-depth characterization of the semi-crystalline structure of iPP, crystallized along different thermodynamic pathways. In the present study we focus on the dependence of the crystal structure and the crystal morphology after fast melt-crystallization which yields non-lamellar crystals. The crystal morphology of iPP was for the first time systematically measured at the nanometer scale as a function of the cooling rate on melt-crystallization in a rather large range between 10^0 and $10^3\,K\,s^{-1}$, using AFM. Within this range of cooling rates, the formation of α-monoclinic structure is replaced by the formation of mesomorphic structure. The transition from formation of α-monoclinic structure to formation of mesomorphic structure occurs between about 10 and 100 $K\,s^{-1}$ (see Fig. 1b), and is paralleled by a transition from a lamellar to a quasi-globular crystal morphology.

Recent analysis of the crystallization temperature as a function of the cooling rate revealed that crystallization occurs at temperatures between 353 and 393 K, if the cooling rate is less than 200 $K\,s^{-1}$, with the crystallization temperature monotonously increasing on decreasing the cooling rate. Crystallization occurred at low temperature between about 293 and 313 K if the cooling rate is between 70 and 1000 $K\,s^{-1}$, with the lower crystallization temperature observed on cooling at higher rate. Crystallization at a rate between 70 and 200 $K\,s^{-1}$, accordingly, revealed two separate crystallization events, occurring at about 353 and 313 K [22]. The results of the present study allow to establish a relation between the

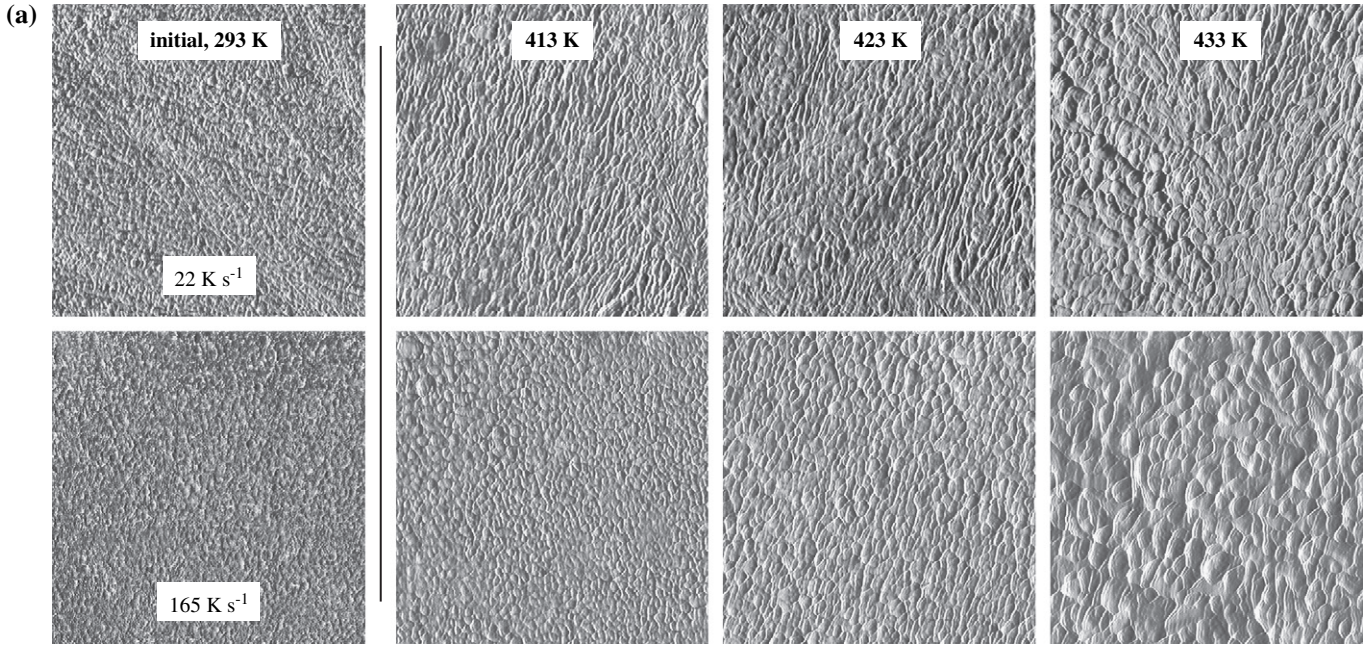

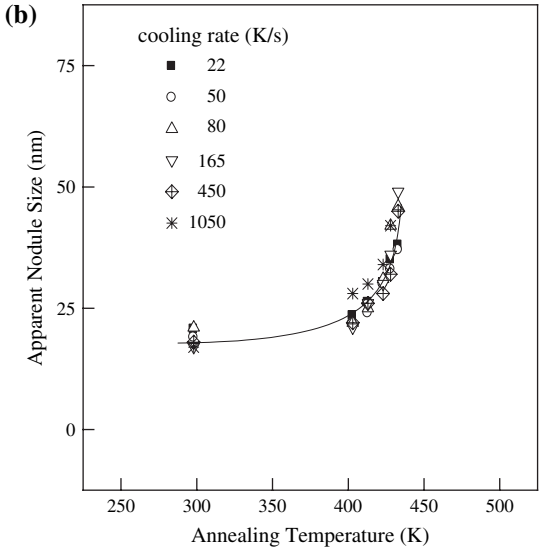

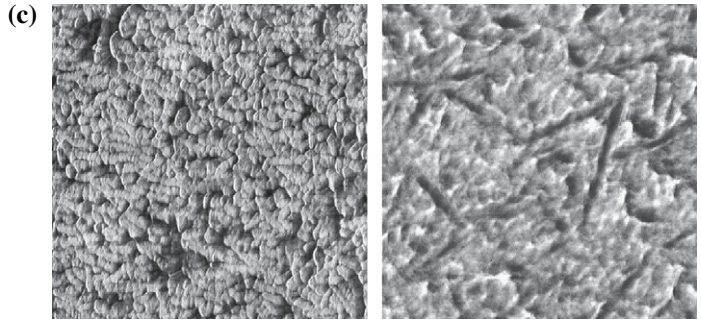

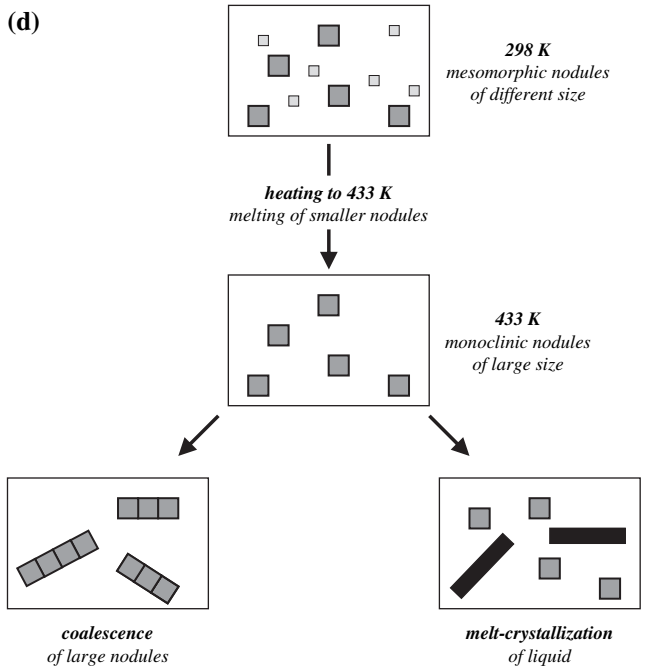

Fig. 3. (a) AFM images of iPP, melt-crystallized at 22 (top) and 165 K s^{-1} (bottom), before annealing (left), and after annealing for a period of 60 min at 413, 423, and 433 K. The size of the AFM images is 1 μm × 1 μm. (b) Size of nodules as a function of the annealing temperature for samples which initially were melt-crystallized at 22, 50, 80, 165, 450 and 1050 K s^{-1}. (c) AFM images of iPP melt-crystallized at 1050 K s^{-1}, after annealing at 433 K for a period of 60 min. The size of the AFM images is 1 μm × 1 μm. (d) Schematic of formation of lamellae on heating mesomorphic nodules to 433 K.

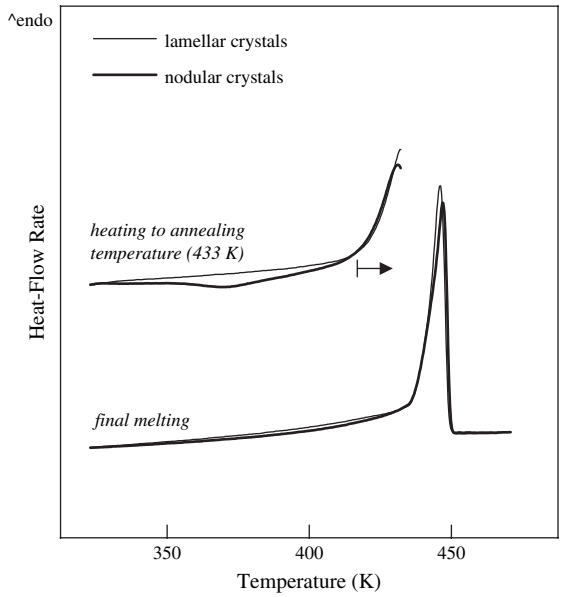

Fig. 4. Heat-flow rate as a function temperature on heating lamellar and nodular crystals of iPP. The upper two curves show the approach of the annealing temperature, and the lower two curves represent final melting after annealing and cooling to ambient temperature.

crystal structure and crystal morphology to the different crystallization events, detected at different temperatures on cooling. The observation of two crystallization processes within a single cooling experiment yields coexistence of monoclinic lamellar and mesomorphic nodular crystals (see Figs. 1b and 2, and Table 1). Application of a sufficiently high rate of cooling between 10^2 and 10^3 K s^{-1} suppresses crystallization at high temperature, which results in exclusive formation of nodular domains with an internal mesomorphic structure. Note that we are not concerned about the minor mismatch of the range of cooling rates where different processes were detected, since different sample preparation yields to specific uncertainties which were not quantified at present. In fact a transition from a twofold crystal morphology to a single crystal morphology occurs at about 10^2 K s^{-1}.

The change of the spherulitic superstructure with increasing cooling rate on melt-crystallization (Fig. 2c) is an experimental confirmation of results of a previous study [34]. The number and size of the spherulites decrease with increasing rate of cooling, which goes parallel to the increase of (a) the fraction of mesomorphic crystals (see Fig. 1b), and (b) the fraction of crystals of quasi-globular shape (see Fig. 2). We assume therefore that within spherulites there is preferred occurrence of lamellar and monoclinic crystals, and that the mesomorphic domains are located within the birefringent matrix. The existence of isolated spherulites in specimens which were crystallized at high cooling rate is confirmed by AFM (not shown). Occasionally in these samples even aligned and thin lamellae were detected, supporting the above view. The absence of monoclinic reflections in the X-ray scans likely is due to the low fraction of lamellar crystals with monoclinic arrangement of chains.

The small and mesomorphic domains, according to standard calorimetry and WAXS analyses [26,27], reorganize on heating at molecular level. The internal mesomorphic structure of nodules converts to crystalline monoclinic structure at about 340 K. The AFM images in Fig. 3a (bottom row) provide evidence that the mesomorphic-to-monoclinic transition is not connected with a qualitative change of the crystal morphology. The preservation of the nodular crystal morphology on heating suggests that this phase transition occurs at the nanometer scale within existing domains without prior and complete melting. We speculate that in case of complete melting of mesomorphic nodules, recrystallization would occur in the form of lamellae which are not observed at least at temperatures below about 430 K.

The literature suggests both formation of lamellae from nodules [12] as well as preservation of the quasi-globular crystal shape [10] on heating. The AFM images in Fig. 3a illustrate that the size of nodules increases as a function of the annealing temperature, with the major increase occurring at temperatures above 400 K (see Fig. 3b). Note that at the temperature of the mesomorphic–monoclinic transition at about 340 K the crystal morphology is almost unchanged. We detected lamellae at the best as a result of annealing at 433 K which is far above the mesomorphic–monoclinic transition. Fig. 3c shows that lamellae of different types can be grown. The observation of lamellae, which seem to be composed of aligned nodules (left image in Fig. 3c, left bottom illustration in Fig. 3d) we explain by coalescence of mobile and stable nodules, for reduction of the surface free energy. The mobility of nodules may increase as a result of melting of unstable, smaller and more defective nodules, which increases the fraction of amorphous liquid and removes local stress within the liquid phase, and ultimately leads to the mobilization of the remaining crystals. Evidence for melting of unstable monoclinic nodules is provided by the DSC analysis in Fig. 4 (top curves, bold line), which shows that melting starts at about 410–415 K, indicated with the arrow in Fig. 4. Occasionally we observed isolated lamellae as a result of annealing at identical temperature of 433 K, coexisting with large and non-aligned nodules (right image in Fig. 3c, right bottom illustration in Fig. 3d). These isolated lamellae apparently do not show internal surfaces or a blocky structure. In this case we assume that the formation occurred by regular crystallization from the melt, supported by former melting of unstable nodules. The exact condition for the formation of these different types of lamellae is not identified yet, which requires further research.

Thermal analysis of semi-crystalline iPP with lamellae or nodules revealed identical temperatures of melting (Fig. 4). Apparently there is no effect of the crystal morphology or shape on the thermodynamic stability. The melting temperature of a crystal, T_m, according to the Gibbs–Thomson equation, depends on the bulk specific heat of fusion, Δh^0_m, the crystal dimensions in lateral direction, a and b, and in longitudinal direction, l_c, the equilibrium melting temperature, T^0_m, and the surface free energies at the lateral surfaces and basal planes, σ and σ_e (Eq. (2)):

$$T_m = T^0_m\left[1 - \frac{2}{\Delta h^0_m}\left(\frac{\sigma}{a} + \frac{\sigma}{b} + \frac{\sigma_e}{l_c}\right)\right] \quad (2)$$

T^0_m is defined as the temperature of equivalence of the free enthalpies of the crystalline and liquid phases, and Eq. (2) indicates that melting of an infinite large crystal occurs at T^0_m. The specific bulk heat of fusion, Δh^0_m, depends on the intermolecular forces between chains within the crystal. The melting point depression, ΔT ($= T^0_m - T_m$), is caused by the increase of the free enthalpy of the crystal due to the presence of surfaces. The total surface free energy of a crystal depends on the area and corresponding specific surface free energy of all crystal faces. Eq. (2) frequently is simplified such that the contribution of the lateral surfaces on the melting temperature is neglected. This simplification is allowed only if the area of the basal planes is considerably larger than the area of the lateral surfaces, and if the specific surface free energy of the basal plane is much larger than the specific surface free energy of the lateral surfaces. Both requirements are fulfilled for laterally extended folded-chain lamellae, since the area of the lateral crystal faces is minor compared to the large basal planes, and since the specific free energy of the fold-surface is about (5–10) × the specific free energy of the lateral surfaces [8].

The bulk specific heat of fusion, Δh^0_m, and the equilibrium melting temperature, T^0_m, we consider as being identical for the lamellar and nodular structures, which are observed after crystallization along different pathways. This assumption is justified since the X-ray scans prove exclusive existence of monoclinic crystal structure after heating to 433 K. Information about surface free energies cannot be gained from the experiments of the present study, however, is available in the literature for the lateral surface and the crystal basal plane with the two extremes of perfect fold-surfaces and non-fold-surfaces [37]. The structure and therefore the free energy of the lateral surfaces, we assume, are independent on the path of crystallization. In case of the basal plane, differences between the surface free energies cannot be excluded since it is proven that the path of crystallization affects the number of molecules, which enter or leave the crystal at this particular surface. We expect an increased tendency of formation of folds in initially slowly melt-crystallized iPP, whereas regular folding may not be possible on crystallization at fast cooling, i.e., at high super-cooling. For further discussion of the experimentally observed identical melting temperatures of lamellar and nodular crystals, model calculations were performed using the Gibbs–Thomson equation. Fig. 5 shows the melting temperature of monoclinic iPP crystals of different thicknesses and surface structures as a function of the crystal lateral size. In detail we used the following values for the calculation: $T^0_m = 460.7$ K [38,39], $\Delta h^0_m = 207$ J g^{-1} [38], $\sigma = 1.15 \times 10^{-6}$ J cm^{-2} [37], $\sigma_{e,fold} = 7 \times 10^{-6}$ J cm^{-2} [37], and $\sigma_{e,non\text{-}fold} = 24.7 \times 10^{-6}$ J cm^{-2} [37]. Lateral dimensions of the crystals were assumed to be identical, i.e., $a = b$. The top and center curves are calculated for folded-chain crystals of thickness 40 nm (top) and 25 nm (center), and the bottom curve is calculated for a non-fold crystal of thickness 40 nm. With these curves it is possible to estimate the melting temperatures of the nodular and lamellar crystals, with a geometry as was obtained after annealing at 433 K and cooling to room temperature. We observed equi-axed crystals of size of about $40 \times 40 \times 40$ nm^3 after quenching and subsequent annealing at 433 K (see Fig. 3b). Crystals with a non-fold-surface are expected to melt below 430 K. In case of a regular fold-surface, the melting temperature increases almost to 450 K. The observed thickness of lamellar crystals, obtained by rather slow cooling of the melt to ambient temperature and subsequent annealing at 433 K, is close to 25 nm. With an assumed lateral dimension of 100 nm, a melting temperature of 446 K is estimated.

The calculated melting temperatures for the folded-chain crystals of size $100 \times 100 \times 25$ nm^3 and $40 \times 40 \times 40$ nm^3 agree remarkably with the experimentally observed

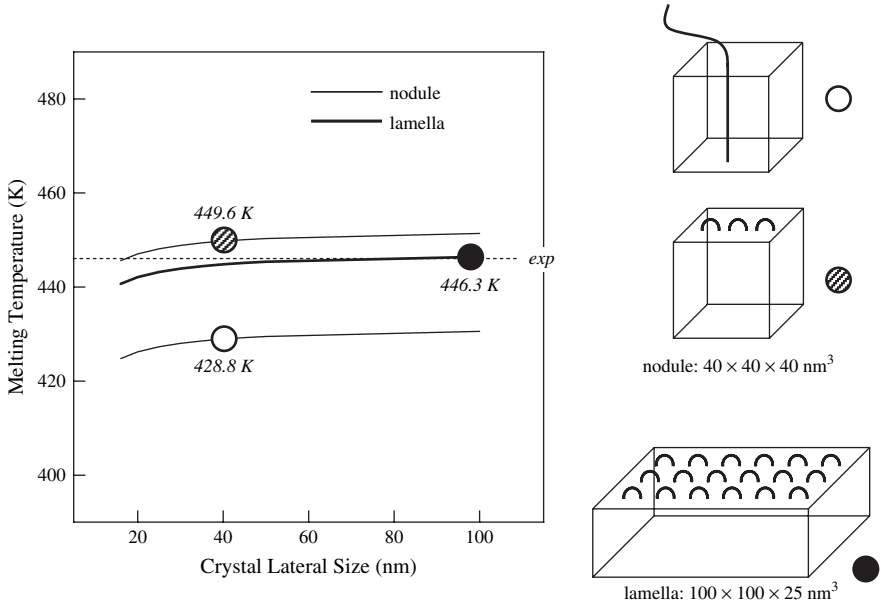

Fig. 5. Melting temperature of fold-surface crystals of 25 nm (center, bold curve) and 40 nm thickness (top curve), and non-fold-surface crystals of 40 nm thickness (bottom curve), as a function of the lateral crystal size. The melting temperatures of the sketched structures are indicated by the symbols. The dotted horizontal line is the experimentally observed melting temperature.

temperature of 446 K. Initially we did not intent to compare absolute values of measured (Fig. 4) and calculated melting temperatures (Fig. 5), rather intended to reduce the comparison to a discussion of melting temperature differences. The exceptional agreement of absolute values, however, points (a) to acceptable morphological analysis, and (b) highly reliable thermodynamic data of iPP crystals (T_m^0, Δh_m^0, σ, σ_e) [37–39]. The data in Fig. 5 suggest that at room temperature nodular and mesomorphic crystals exhibit a fold-surface at the crystal top and bottom planes after annealing at 433 K. The melting point of crystals with a non-fold-surface is about 20 K lower than the observed melting temperature, regardless the lateral dimensions. Furthermore the calculation in Fig. 5 provides the information that the lateral size of the crystals does not largely affect the melting temperature if it is exceeding 30–40 nm. The melting temperature of a crystal of 25 nm thickness (center curve) and 40 nm lateral dimension is 444.8 K. The melting temperature increases only minor to 446.3 K and 447.0 K for crystals of identical thickness with lateral dimensions of 100 nm and 200 nm, respectively. This argument is necessary to explain the rather arbitrary selection of the length of lamellae for comparison of melting temperatures.

5. Conclusions

The morphology of crystals of iPP can be controlled in a rather large range of size and shape by the pathway of crystallization. Non-isothermal melt-crystallization yields nodular mesomorphic crystals of size less than 20 nm if the cooling rate exceeds about 100 K s^{-1}. Melt-crystallization at a rate between 10 and 100 K s^{-1} causes the formation of both lamellar monoclinic crystals and nodular mesomorphic domains. The crystal shape is preserved on annealing at elevated temperature. Lamellar crystals grow in thickness direction, and the initial mesomorphic nodular domains seem to grow in both lateral and longitudinal direction. The mesomorphic-to-monoclinic transition in nodular crystals at about 340 K is not accompanied by complete melting of the domains and recrystallization, rather seems to occur at local scale within existing domains. The domain size is controlled by the maximum annealing temperature, and can reach values twice the initial size. Annealing at temperatures within the melting range allows formation of lamellae by coalescence of nodules, evidenced by a distinct blocky structure of lamellae, and by recrystallization from the liquid state. Experimental analysis of the melting behavior reveals identical thermodynamic stability of nodular and lamellar crystals after annealing at 433 K. Model calculations, based on experimentally observed morphological data, prove identical surface free energies of nodular and lamellar crystals.

Acknowledgment

This research was partially supported by funding from the ministry of culture of Saxony-Anhalt (Germany), and by a STSM grant within the EU COST-P12 program for one of the authors (Q.Z).

References

[1] Wunderlich B. Crystal structure, morphology, defects. In: Macromolecular physics, vol. 1. New York: Academic Press; 1973.
[2] Strobl G. The physics of polymers. Berlin: Springer; 1996.
[3] Storks KH. J Am Chem Soc 1938;60:1753–61.
[4] Keller A. Philos Mag 1957;2:1171–5.
[5] Fischer EW. Z Naturforsch 1957;12a:753–4.
[6] Mathot VBF, Scherrenberg RL, Pijpers TFJ. Polymer 1998;39:4541–59.
[7] Herrmann K, Gerngross O, Abitz W. Z Phys Chem 1930;B10:371–94.
[8] Hoffmann JD, Davis GT, Lauritzen JI. The rate of crystallization of linear polymers with chain folding. In: Hannay HB, editor. Crystalline and noncrystalline solids. Treatise on solid state chemistry, vol. 3. New York: Plenum Press; 1976.
[9] Zachmann HG. Kolloid ZZ Polym 1967;216–217:180–91.
[10] Hsu CC, Geil PH, Miyaji H, Asai K. J Polym Sci Polym Phys Ed 1986;24:2379–401.
[11] Ogawa T, Miyaji H, Asai K. J Phys Soc Jpn 1985;54:3668–70.
[12] Wang ZG, Hsaio BS, Srinivas S, Brown GM, Tsou AH, Cheng SZD, et al. Polymer 2001;42:7561–6.
[13] Grubb DT, Yoon DY. Polym Commun 1986;27:84–8.
[14] Caldas V, Brown GR, Nohr RS, MacDonald JG, Raboin LE. Polymer 1994;35:899–907.
[15] McAllister PB, Carter TJ, Hinde RM. J Polym Sci Polym Phys Ed 1978;16:49–57.
[16] Bodor G, Grell M, Kallo A. Faserforsch Textiltechnik 1964;15:527–34.
[17] Miyamoto Y, Fukao K, Yoshida T, Tsurutani N, Miyaji H. J Phys Soc Jpn 2000;69:1735–40.
[18] Minami S, Tsurutani N, Miyaji H, Fukao K, Miyamoto Y. Polymer 2004;45:1429–32.
[19] Martorana A, Piccarolo S, Scichilone F. Macromol Chem Phys 1997; 198:597–604.
[20] Piccarolo S, Alessi S, Brucato V, Titomanlio G. Crystallization of polymers. In: Dosiere M, editor. NATO ASI Ser Ser C Math Phys Sci. Kluwer; 1993. p. 475–80.
[21] Adamovsky SA, Minakov AA, Schick C. Thermochim Acta 2003; 403:55–63.
[22] De Santis F, Adamovsky S, Titomanlio G, Schick C. Macromolecules 2006;39:2562–7.
[23] Gradys A, Sajkewicz P, Minakov AA, Adamovsky S, Schick C, Hashimoto T, et al. Mater Sci Eng A 2005;413–414:442–6.
[24] Natta G, Peraldo M, Corradini P. Rend Acc Naz Lincei 1959;26:14.
[25] Natta G, Corradini P. Nuovo Cimento 1960;15(Suppl):40.
[26] Fichera A, Zannetti R. Makromol Chem 1975;176:1885–92.
[27] Zannetti R, Celotti G, Fichera A, Francesconi R. Makromol Chem 1969;128:137–42.
[28] Androsch R, Wunderlich B. Macromolecules 2001;34:5950–60.
[29] Androsch R, Wunderlich B. Macromolecules 2001;34:8384–7.
[30] Basell Bayreuth Chemie GmbH. Private communication; 2001.
[31] Brucato V, Piccarolo S, La Carubba V. Chem Eng Sci 2002;57:4129–43.
[32] Brandrup J, Immergut EH, Grulke EA. Polymer handbook, vol. 1. Hoboken: Wiley – Interscience; 1999.
[33] Wunderlich B. Thermal analysis of polymeric materials. Berlin: Springer; 2005.
[34] Piccarolo S. J Macromol Sci Phys 1992;B31:501–11.
[35] Norton DR, Keller A. Polymer 1985;26:704–16.
[36] Bassett DC, Olley RH. Polymer 1984;25:935–43.
[37] Cheng SZD, Janimak JJ, Zhang A, Cheng HN. Macromolecules 1990;23:298–303.
[38] Bu HS, Cheng SZD, Wunderlich B. Makromol Chem Rapid Commun 1988;9:75–7.
[39] Wunderlich B. Crystal melting. In: Macromolecular physics, vol. 3. New York: Academic Press; 1980.